JOURNAL OF SPACECRAFT AND ROCKETS
Vol. 31, No. 4, July–August 1994

Radiation Control with Selectively Reflective Overcoats

Susan M. White*
NASA Ames Research Center, Moffett Field, California 94035

Selectively reflective overcoats can be used to significantly reduce the temperature of a heated surface under conditions where short-wavelength radiation is the predominant mode of heat transfer to the surface and the total heating is below the melting or ablation limit. In addition, these overcoats can be used to detect and characterize radiation. Theoretical models are used to predict the optical properties of selectively reflective overcoats on an opaque substrate, such as metal or reaction-cured glass. The computed surface reflectance is compared with experimental data. The predicted optical properties of selectively reflective overcoats are used to compute the reduction in surface temperature attainable with this strategy. Design curves are presented for investigating selectively reflective overcoats of different materials.

Nomenclature

A = absorption coefficient
a = absorption, m^{-1}, series coefficient
B = backscatter fraction
b = series coefficient
c = separation between particles, m
d = particle diam, m
e = blackbody function, $W/m^2 \cdot \mu m$
f_v = solid-volume fraction
I = intensity, $W/m^2 \cdot \mu m \cdot sr$
K = temperature, K
m = complex refractive index
n = summation index
N = particle size distribution function
P = Legendre polynomial
p = percentage of energy scattered into a solid angle
Q = efficiency
q = heat flux, W/m^2
R = reflectance
r = distance, m
T = transmittance
x = distance, m
α = size parameter $\pi d/\lambda$
γ = variable defined in Eq. (14)
δ = variable defined in Eq. (15)
ϵ = emittance
θ = angle from incident direction
λ = wavelength, μm
μ = $\cos\theta$
σ = Stefan-Boltzman constant, $W/m^2 \cdot K^4$
$\bar{\sigma}$ = scattering coefficient, m^{-1}
ϕ = angle
Υ = Neumann Riccati-Bessel function
ψ = Bessel Riccati-Bessel function

Superscripts

$+$ = forward direction
$-$ = backward direction
$\sim$ = corrected for size distribution and dependence

Subscripts

a = absorption
b = blackbody function
c = convective heating
d = dependent scattering
e = effective
i = independent scattering
j = integration variable
r = radiative heating
s = scattering
1 = medium or component 1
2 = medium or component 2

Presented as Paper 91-1320 at the AIAA 26th Thermophysics Conference, Honolulu, HI, June 24–26, 1991; received Feb. 8, 1993; revision received July 27, 1993; accepted for publication July 28, 1993.

*Research Scientist, Thermal Protection Materials Branch. Member AIAA.

Introduction

SHOCK-LAYER radiation is expected to contribute a significant portion of the heat transfer to the new generation of atmospheric entry vehicles, the aeroassisted space transfer vehicles (ASTVs).[1–3] Because the incident radiative flux is concentrated in the ultraviolet range[4] and the vehicle surface is designed to emit primarily in the infrared range, one very efficient strategy for thermal protection of such a surface involves reflecting back the ultraviolet radiation while maintaining a high emittance in the infrared region. This strategy reduces the radiative heat flux to, and the temperature of, the vehicle surface. As a result, the weight and thickness of the insulation material required to protect the vehicle can be reduced, while maintaining the operating temperature within acceptable limits. The concept is applicable at temperatures below the melting or ablation limits of the overcoated surface, when the ratio of the radiative to the convective heating rates is sufficiently large.

The radiation incident on a surface always has a spectral distribution characteristic of its source and the transmission, absorption, or emission of the intervening media. In most cases of interest, the incident energy is concentrated in a specific wavelength region or set of bands. In the application discussed here, the ultraviolet contributes the major component of the incident radiant energy. Shock-layer radiation heavily weighted to the ultraviolet is characteristic of high-speed entry of a blunt vehicle into a planetary atmosphere, or from a high-temperature blackbody source. A selective surface overcoat can be designed having a high reflectance in the wavelength range where the incident energy is concentrated, while maintaining the high emittance of an appropriate substrate in the infrared, where the overcoat layer is relatively transparent.

The concept of selectively reflecting part of the incident radiation has been explored in the past[5,6] and continues to be of interest in specialized applications. A selectively reflective surface composed of an overcoat of high-temperature ceramic particles on a high-emittance substrate can reflect in excess of 80% of the incident radiation at wavelengths smaller than its cutoff wavelength, and

transmit most of the radiative energy above that wavelength. The optical properties of such an overcoat substrate composite depends on many variables: the particle shape, the solid-volume fraction, the size distribution of the particles, and, at each wavelength, the size parameter and the material optical properties of the particles and the substrate. Most of these parameters can be controlled, by the proper choice of manufacturing techniques or by material selection, in order to tailor an overcoat substrate system for a wide variety of applications. The predictive model developed below can be applied to other materials and configurations, and used as a design tool to parametrically study the use of particulate overcoats layered on substrates.

Spectrally selective reflective overcoats can be used to lower the temperature of a surface, but the melting temperature of the overcoat and the substrate are limiting temperatures. Physically, reflection occurs at the many interfaces between the particles and the surrounding medium. However, melting destroys that interface, and the reflectance decreases accordingly. Embedding the reflective particles in a more refractory medium will extend the useful temperature range, but will decrease the overall reflectance. The reflectance decreases because reflection at an interface between two media is governed by the ratio of the real parts of the refractive indices. This ratio is maximized when the particles are surrounded by vacuum or a gas, rather than embedded in a solid. It is maximized because the refractive index of vacuum has the minimum possible value: 1. The refractive indices of air and other gases fall within 1% of 1. In contrast, the real part of the refractive index of a typical liquid is 1.3. For solids, the refractive index typically falls between 1.5 and 3.5. There are exceptional materials; for example, extremely low-density porous aerogels have refractive indices more typical of gases than of solids. The surrounding medium is assumed below to have a refractive index of 1, but this is not a limiting assumption. It is only necessary to replace the refractive index m in the analysis by the ratio of the refractive indices of the coating and the surrounding media, and to account for reflectance at the outer boundary, to utilize the model developed below for an embedded coating.

Analysis

Mie scattering theory is used to calculate the reflective properties of each particle.[7–10] The particle size influences the scattering of light through the size parameter $\alpha = \pi d/\lambda$, which is the particle size scaled by the wavelength. The two-flux model[11,12] predicts the radiative properties of a layer of such particles. The model is corrected for dependent scattering effects.[13–18] The integrated average of the radiative properties, weighted by the particle size distribution, accounts for the effect of different particle sizes on scattering. Because the overcoats were very thin, they were assumed to be isothermal.

The particles making up the overcoat are assumed to be spheres, of a known size distribution. As discussed by Siegel and Howell,[9] assuming a spherical shape is valid for most irregular-shaped particles. The scattering characteristic of a single sphere is a well-known function of the size parameter and the optical properties of the material. The size parameter α is the scaled particle size, and it covers a wide range in these calculations. A typical particle size for this application is 0.5 μm, and the wavelengths considered range from the infrared at 15.0 μm through the visible to the ultraviolet at 0.25 μm, so that the size parameter ranges over two orders of magnitude. The scattering coefficients Q_a and Q_s are calculated directly from Mie theory using a program developed by Bohren and Huffman,[10] rather than utilizing the simpler approximate expressions applicable only to the extreme cases of small-particle Rayleigh scattering ($\alpha \ll 1$) or the geometrical optics domain of large, diffuse particles ($\alpha \gg 1$). The particles are assumed to be diffuse reflectors.

Solving Maxwell's equation in spherical coordinates gives the components of radiation polarized in two perpendicular planes in terms of Legendre polynomials P and Riccati-Bessel functions Ψ and Υ, based on the half-order Bessel functions and the Neumann functions, respectively, and the first derivatives thereof in the following classical expressions[8]:

$$I_1 = \frac{\lambda^2}{4\pi^2 r^2}\sin^2\phi \times \sum_{n=1}^{\infty}\left[\frac{2n+1}{n(n+1)}\left(a_n\frac{P_n^{(1)}(\cos\theta)}{\sin\theta} + b_n\frac{\mathrm{d}P_n^{(1)}(\cos\theta)}{\mathrm{d}\theta}\right)\right]^2 \quad (1)$$

$$I_2 = \frac{\lambda^2}{4\pi^2 r^2}\cos^2\phi \times \sum_{n=1}^{\infty}\left[\frac{2n+1}{n(n+1)}\left(a_n\frac{\mathrm{d}}{\mathrm{d}\theta}P_n^{(1)}(\cos\theta) + b_n\frac{P_n^{(1)}(\cos\theta)}{\sin\theta}\right)\right]^2 \quad (2)$$

where

$$a_n = \frac{\Psi_n(2\alpha)\Psi_n'(\alpha m) - m\Psi_n(\alpha m)\Psi_n'(2\alpha)}{\Upsilon_n(2\alpha)\Psi_n'(\alpha m) - m\Psi_n(\alpha m)\Upsilon_n'(2\alpha)} \quad (3)$$

$$b_n = \frac{m\Psi_n(2\alpha)\Psi_n'(\alpha m) - \Psi_n(\alpha m)\Psi_n'(2\alpha)}{m\Upsilon_n(2\alpha)\Psi_n'(\alpha m) - \Psi_n(\alpha m)\Upsilon_n'(2\alpha)} \quad (4)$$

Here, λ is the wavelength in vacuum, and m is the refractive index of the particulate medium. For unpolarized incident radiation, the intensity is given by the average of the two polarized components,

$$I = (I_1 + I_2)/2 \quad (5)$$

Treating the particulate overcoat as an absorbing/scattering medium, the equation of transfer for a plane-parallel slab geometry without emission and experiencing diffuse incident radiation is

$$\mu\frac{\mathrm{d}I}{\mathrm{d}x} = -(\bar{\sigma}+\bar{a})I + \frac{\bar{\sigma}}{2}\int_{-1}^{1} I(\alpha,\mu_j)p(\mu,\mu_j)\,\mathrm{d}\mu_j \quad (6)$$

using the shorthand notation $\mu = \cos\theta$, and where μ_j is the dummy variable of integration.

The bulk scattering and absorption coefficients are as follows:

$$\bar{\sigma} = 3BQ_s f_v/d \quad (7)$$

$$\bar{a} = 3Q_a f_v/d \quad (8)$$

where the backscatter fraction B is given by integrating over the backward-facing hemisphere the function p, the percentage of the incident radiation scattered into a given solid angle,

$$B = \frac{1}{2}\int_0^1\int_{-1}^0 p(\mu,\mu_j)\,\mathrm{d}\mu\,\mathrm{d}\mu_j \quad (9)$$

The overcoat layer itself is modeled using a two-flux model. This well-known approach is taken by assuming a semi-isotropic phase function, and integrating over the forward (+) and backward (−) hemispheres gives

$$\frac{\mathrm{d}I^+}{\mathrm{d}x} = -(\bar{\sigma}+\bar{a})I^+ + \bar{\sigma}I^- \quad (10)$$

$$\frac{\mathrm{d}I^-}{\mathrm{d}x} = +(\bar{\sigma}+\bar{a})I^- - \bar{\sigma}I^+ \quad (11)$$

The derivation of a closed-form solution for the reflectance R or transmittance T through a plane layer governed by the two-flux model[13–15] is expressed in terms of the absorption coefficient $\bar{a}$ and the scattering coefficient $\bar{\sigma}$, in terms of the variables

$$\gamma = [\bar{a}(\bar{a}+2\bar{\sigma})]^{\frac{1}{2}} \quad (12)$$

$$\delta = [\bar{a}/(\bar{a}+2\bar{\sigma})]^{\frac{1}{2}} \quad (13)$$

The transmittance through a particulate layer is given by

$$T_1 = \frac{2\delta}{(1+\delta^2)\sinh(\gamma L) + 2\delta\cosh(\gamma L)} \tag{14}$$

and the reflectance of such a layer is given by

$$R_1 = \frac{(1-\delta^2)\sinh(\gamma L)}{(1+\delta^2)\sinh(\gamma L) + 2\delta\cosh(\gamma L)} \tag{15}$$

The scattering by one particle can be considered independent of the scattering by the surrounding particles only if the spacing between the particles is large enough to reduce the interference due to phase addition and cancellation between the scattered fields. Experimental data give two criteria to differentiate between independent and dependent scattering: the size parameter and the solid-volume fraction or packing factor f_v. These parameters determine the ratio of the interparticle clearance c to the wavelength of incident light. Assuming rhombohedral packing of perfect spheres gives the following expression for the spacing parameter of the medium:

$$c/\lambda = (\alpha/\pi)(0.9047/f_v^{\frac{1}{3}} - 1) \tag{16}$$

The domains of independent and dependent scattering by spherical particles were defined by Drolen, Kumar, and Tien.[16–18] The following empirical correlation[13] is used to compensate for dependent scattering effects:

$$\log[\log(Q_{s,i}/Q_{s,d})] = 0.25 - 5.1(c/\lambda) \tag{17}$$

Multiple scattering effects are not taken into consideration in this analysis.

In modeling particulate overcoats, it is important to take into account the particle size distribution function $N(r)$, where r represents the particle diameter. After the scattering efficiency Q_s and the absorption efficiency Q_a are calculated from Mie theory, the scattering and absorption efficiencies are corrected for dependent scattering effects if necessary, weighted by the particle size distribution function, and integrated over all particle sizes. Changing the order of these steps did not measurably affect the outcome of the final calculations. The particle size weighted average of the efficiency factors is calculated as follows:

$$\tilde{Q} = \frac{\int_0^\infty Q(r)N(r)\,dr}{\int_0^\infty N(r)\,dr} \tag{18}$$

The tilde is used to emphasize that the scattering efficiencies and all derived quantities have been corrected for particle size distribution and for dependent scattering effects.

Solving for the overall reflectance of a layer applied to an opaque substrate having a spectral hemispherical emittance ϵ_2 yields the following expression for the effective reflectance of the composite surface:

$$\tilde{R}_e(\lambda) = \frac{\tilde{R}_1(\lambda) + [1-\epsilon_2(\lambda)][1-2\tilde{R}_1(\lambda)]\tilde{T}_1^2(\lambda)}{1-[1-\epsilon_2(\lambda)]\tilde{R}_1(\lambda)\tilde{T}_1^2(\lambda)} \tag{19}$$

The reflectance, transmittance, and emittance in Eq. (19) are spectral quantities, and the dependence on wavelength is shown explicitly for emphasis. In applying this model to a spectrally selective overcoat on an ideal gray substrate, the substrate emittance ϵ_2 would be a constant.

The parameters governing the radiative properties of a particulate overcoat on a substrate can be divided into two categories: the material optical properties, through the complex index of refraction m, which depends upon the material, purity, temperature, and wavelength; and the geometric properties of the layer, i.e., the particle size d, the solid-volume fraction f_v, and the layer thickness l.

The following calculations were made using alumina, titania, and silica particles for the overcoat material. The bulk optical properties were taken from Palik[19] or Malitson[20] when possible, or were calculated from transmittance data from Touloukian and DeWitt[21] and from absorption coefficient data from Driscoll.[22] Parry and Brewster[23] summarized previous work and presented new high-temperature measurements for alumina. In addition, Toon and Polack[24] and Goodwin and Mitchner[25] presented optical-property information on alumina and reviewed the literature. This analysis is limited by the uncertainty in the optical properties.

Calculations were made assuming radiative equilibrium of the surface. This decouples the heat transfer from the flow and implies that the surface comes to a steady-state temperature by emitting all the absorbed convective and radiative energy to an energy sink. Radiative equilibrium was assumed so that one could make straightforward comparisons between different overcoats and could make parametric studies. The absorption of a spectrally selective overcoat is an integrated average weighted by the incident spectral radiant energy,

$$A = \frac{1}{q_r}\int_0^\infty [1-\tilde{R}_e(\lambda)]q_r(\lambda)\,d\lambda \tag{20}$$

An energy balance on the opaque surface that is composed of the overcoat on an RCG substrate gives

$$\epsilon\sigma K_s^4 = Aq_r + q_c \tag{21}$$

where the emittance is a function of the surface temperature and is given by

$$\epsilon = \frac{1}{\sigma K^4}\int_0^\infty [1-\tilde{R}_e(\lambda)]e_b(\lambda)\,d\lambda \tag{22}$$

for the opaque surface. Equations (20) through (22) can be solved iteratively for the surface temperature.

Results

The results show that using a selectively reflective overcoat alters the surface optical properties so as to reduce the surface temperature significantly. However, there is a tradeoff between the three coupled competing effects of reflectance, emittance, and catalyticity. Increasing the surface reflectance decreases the energy absorbed by the surface. Decreasing the surface emittance reduces the efficiency of reradiation. Altering the surface catalyticity by the presence of the overcoat may increase the surface convective heat flux. Under less than ideal conditions (specifically, under low levels of short-wavelength radiative heat flux) the overcoated RCG surface would reach a higher temperature than an uncoated RCG surface, because the overcoat would lower the surface emittance without sufficiently reducing the absorbed radiant energy.

Figure 1 shows the spectral reflectance of 5.0-μm-thick layers composed of identically sized alumina particles. The sharp spectral features occur at specific values of the size parameter α. The maximum reflectance for each particle size occurs at a wavelength that increases with increasing particle size. Because the refractive index of the material itself changes with wavelength, the overall reflectance changes, so that the curve changes shape while it shifts to longer wavelengths.

Figures 2–4 show the calculated reflectance for different layer thicknesses for several different materials. Figure 2 gives the calculated reflectance results for alumina particles in a silica matrix, to illustrate the effect of embedding the particulate material in a solid matrix rather than surrounding the alumina particles with air or vacuum. This approach has several significant benefits. A more refractory material can be used for the surrounding medium, or a lower particle density can be attained by dispersing the scattering particles in the embedding medium. The surrounding medium, however, must exhibit a low absorption in the spectral region where the incident energy should be reflected. Figure 2 illustrates that embedding the overcoat particles in a surrounding medium has the additional benefit of sharpening the cutoff feature.

Figure 3 shows the reflectance calculated as a function of wavelength for three thicknesses of particulate overcoats of 0.5-μm-diam silica-glass particles on an opaque layer of low-emittance reaction-cured glass (RCG). The reflectance of such overcoats is controlled by several independent factors: the geometry of particles arrayed in a slab layer over an opaque slab, the particle size distribution,

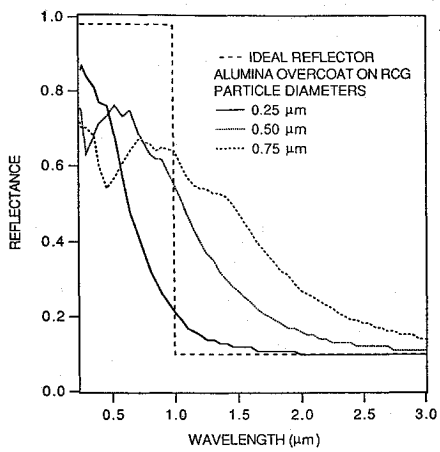

Fig. 1 Spectral reflectance of a 5.0-μm-thick alumina overcoat on RCG and an ideal overcoat.

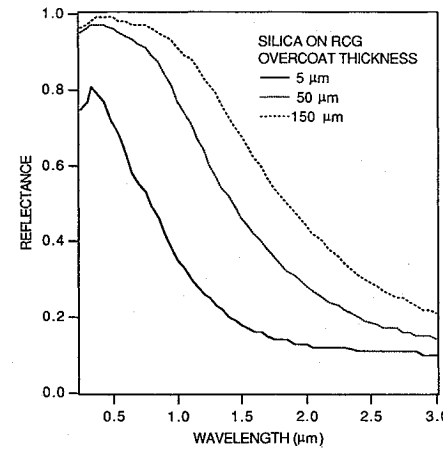

Fig. 3 Spectral reflectance of different thicknesses of 0.5-μm silica glass overcoats on RCG coating.

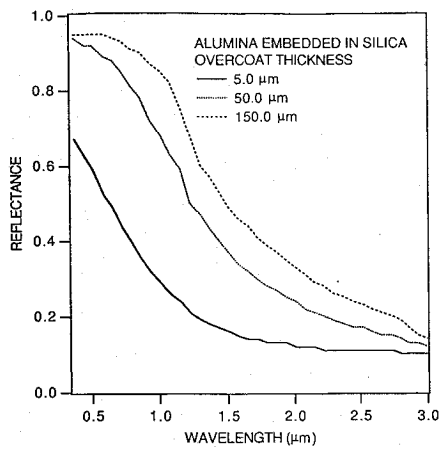

Fig. 2 Spectral reflectance of 0.5-μm alumina particles embedded in a silica matrix on RCG.

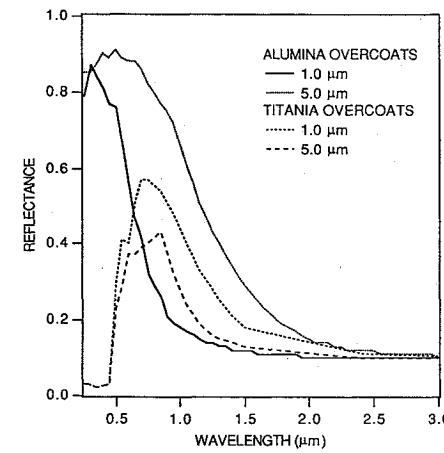

Fig. 4 Spectral reflectance of very thin alumina and titania overcoats on RCG coating.

the refractive index of the particle material and the surrounding medium, and the properties of the underlying substrate. Different materials show similar trends: For silica, alumina, and titania overcoats on RCG, the thinner layers have a lower overall reflectance and a sharper cutoff in reflectance. An energy balance will result in lower surface temperatures for the thinner overcoats than for the thicker overcoats. The advantage of the thinner overcoats is apparent from these calculations.

Figures 1–4 illustrate the advantage of using small particles in thin layers to obtain sharp cutoffs in the short-wavelength region of the spectrum. Figure 4 shows the reflectance calculated for extremely thin overcoat layers of alumina and of titania. The alumina overcoats exhibit desirable features for this application: a sharp cutoff and a high short-wavelength reflectance. The titania overcoats do not exhibit the high reflectance in the short-wavelength region or the sharp cutoff useful for this application. Consequently, this material can be ruled out as a candidate, based on these numerical experiments. These results illustrate the power of this method when reliable material properties are available.

Figures 1–4 give results for monosize particles, which could be obtained with carefully controlled processing and sieving. However, a wide range of particle sizes can easily be obtained. Ball-milling produces a range of small particles and yields a characteristic symmetrical bell-shaped distribution of particle sizes. Different processing techniques or a series of sieving steps will result in different particle size distributions, which may be advantageous for enhancing certain characteristics of an overcoat. The effective scattering coefficients must be weight-averaged to yield an appropriate value for the scattering coefficient of the mixture. For the conditions under consideration here, the scattering coefficient was not sensitive to the precise shape of the particle size distribution curve used, as long as a wide range of particle sizes was present. An exponential distribution yielded almost indistinguishable results from a symmetrical bell-shaped distribution.

Figure 5 shows that the sharp spectral features seen in overcoats composed of uniform-sized particles are averaged out to a smoother curve by a weight-averaged distribution of particle sizes. Figure 5 shows the effect of increasing the thickness of an overcoat with the assumed normal size distribution. Decreasing the overcoat thickness results in a lower reflectance and a sharper cutoff feature located at a shorter wavelength. This desirable feature must be weighed against the durability of such an overcoat as well as the difficulty of application and reproducibility.

The total hemispherical emittance given in Eq. (22) for the alumina-overcoated surface is plotted as a function of the temperature of equivalent blackbody radiation in Fig. 6. The surface reflectance for incident radiation having the spectral distribution of a blackbody can be calculated from this plot. Particle-size-weighted values were used with a mean particle size of 0.5 μm.

Figure 7 shows the results of a set of parametric calculations for different ratios of radiative heating to the total heating rate. The effect of the spectral composition of the incident radiation is illustrated by varying the predominant wavelength range on the surface temperature of the alumina-overcoated RCG surface. The results are shown plotted as a function of the temperature difference between an RCG surface and an overcoat of alumina particles on an RCG substrate. When short-wavelength radiation predominates, as when the radiation is emitted by a high-temperature source (e.g., a highly energetic shock layer), the coatings having a short-wavelength cutoff efficiently reflect a large portion of the radiative energy without significantly reducing the surface emittance, and a lower surface temperature results. When longer-wavelength incident radiation

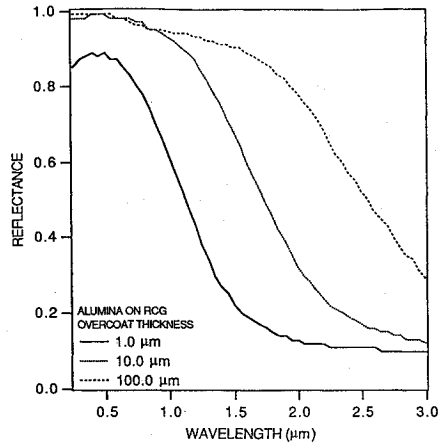

Fig. 5 Particle-size-averaged reflectance of alumina overcoat on RCG coating as a function of peak wavelength of radiation.

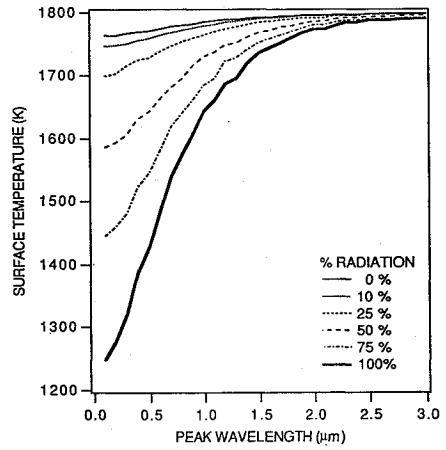

Fig. 7 Temperature of a 10-μm-thick alumina overcoated RCG for different ratios of radiative to total incident heat flux.

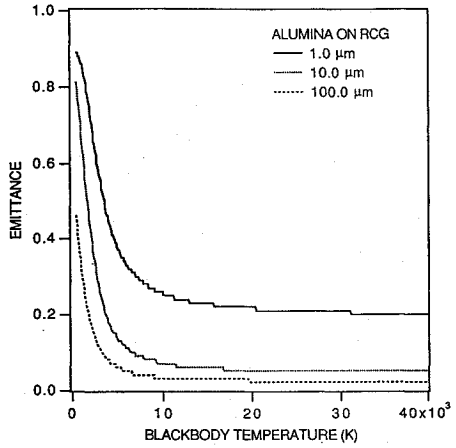

Fig. 6 Particle-size-averaged total emittance vs. temperature of incident blackbody radiation of alumina overcoats on RCG.

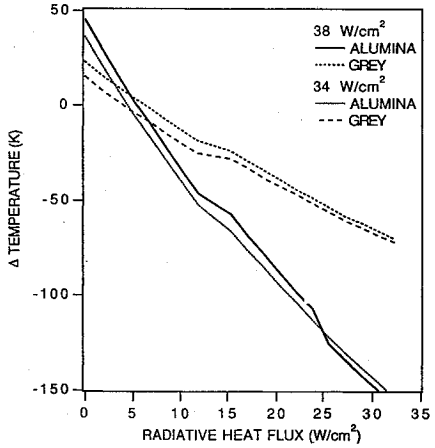

Fig. 8 Temperature difference between an uncoated RCG surface and alumina-overcoated RCG or 50% gray overcoat.

predominates, the coating exhibiting the cutoff in reflectance essentially lowers the surface emittance without significantly reducing the radiative heat load absorbed, so a higher surface temperature results.

The different curves in Fig. 7 show the radiative heating at varying percentages of the total heating load. The benefits of using a selective reflector are apparent from this figure, and the magnitude of the possible reduction in surface temperature can be read directly from this plot.

A specific application is shown in Fig. 8 for two heating rates, 34 W/cm^2 (30 Btu/ft^2 · s) and 38 W/cm^2 (34 Btu/ft^2 · s), with a range of radiative heat fluxes up to 11 W/cm^2 (10 Btu/ft^2 · s). Figure 8 illustrates graphically the change in the surface temperature resulting from the application of a coating of this class. The results shown are plotted as a function of the temperature difference between an RCG surface and an overcoat of alumina particles on an RCG substrate. For purposes of comparison, the temperature difference for a gray overcoat, having a constant reflectance of 50%, is shown. The overcoated RCG surface exhibits the short-wavelength cutoff phenomenon illustrated in the previous figures. These calculations were made on a 10-μm-thick layer of alumina particles, having a mean particle diameter of 0.5 μm. The incident radiation was assumed to be blackbody radiation, scaled to give the desired surface heat flux, with a peak at 0.5 μm. In all cases, a nearly linear variation of the temperature difference between the surface temperature of the uncoated RCG surface and the overcoated RCG surface can be seen. The local slopes of the curves depend on the spectral optical properties of the overcoated surfaces. The alumina overcoat curves show steeper slopes than the gray reflector curves in both cases. This yields an immediate payoff to experimentalists, because the temperature difference between an uncoated and an overcoated surface is large enough to be measured reliably with differential thermocouples.

Figure 9 illustrates the dramatic decrease in surface temperature attainable using an alumina overcoat on an RCG surface under the appropriate conditions. These calculations represent the difference in surface temperature between an uncoated RCG surface and an alumina-overcoated RCG surface. A negative value for the temperature difference represents an improvement in thermal performance through a decrease in surface temperature. This advantage is seen most clearly when radiation contributes a large fraction of the incident energy flux. At lower levels of incident radiation, an inversion occurs. The overcoated surface exhibits a higher temperature than an RCG surface subject to the same incident flux. This occurs because the surface emittance has been lowered by the overcoat, and insufficient energy can be reflected to compensate for the lower emittance. However, the strategy pays off as the ratio of radiative to total heat flux is increased, and a significant lowering of the temperature of the overcoat surface is seen. At 40% radiative heating, the overcoated surface has a lower temperature at total heat fluxes below approximately 45 W/cm^2 (40 Btu/ft^2· s), so the application of an overcoat would be useful in this range of surface heating rates. At higher ratios of radiative to total heating, there is always a payoff on applying a selectively reflective overcoat, in that one obtains a lower surface temperature. The payoff can, theoretically, be extremely high, attaining a value of nearly 1000 K in the most extreme case given. The decreased surface temperatures are possible only up to the melting temperatures of the overcoat and substrate materials. These calculations were made for a 10-μm-thick layer of alumina particles, having a mean particle diameter of 0.5 μm, subject to incident radiation having a peak at 0.25 μm in the ultraviolet.

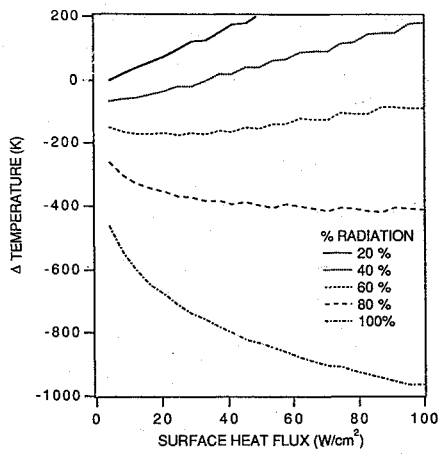

Fig. 9 Temperature difference between an RCG surface with and without an alumina overcoat.

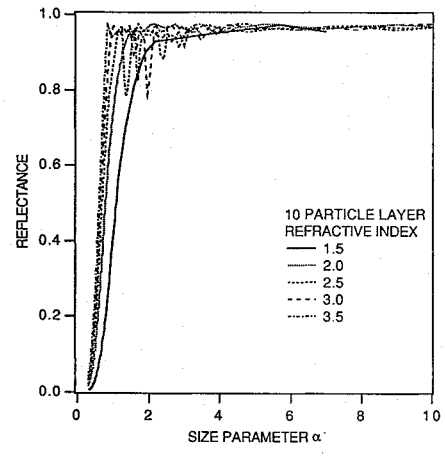

Fig. 11 Comparison of five refractive indices for 10-particle-thick overcoats.

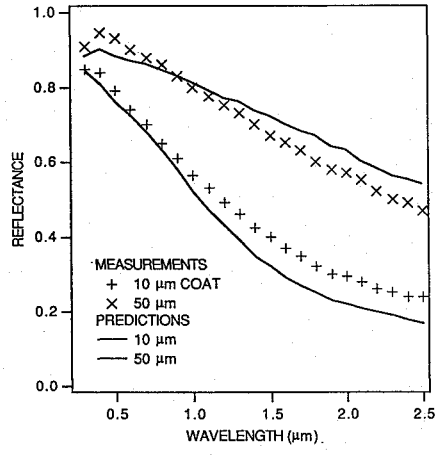

Fig. 10 Experimental measurements and calculated spectral reflectance for alumina overcoats on RCG.

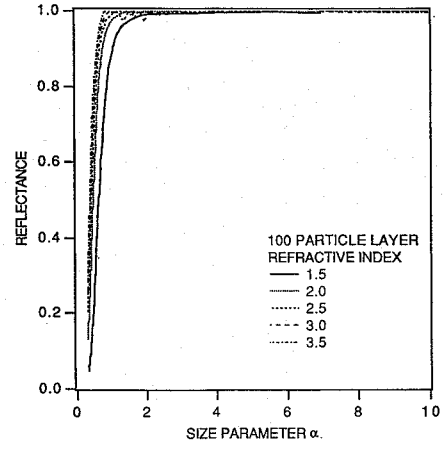

Fig. 12 Comparison of five refractive indices for 100-particle-thick overcoats.

Figure 10 shows that the reflectance measured for two overcoated samples follows the trends predicted for these selectively reflective overcoats. The predictions for the peak reflectance, cutoff features, and overall shape of the reflectance curves are reproduced in the experimental data. As expected, the peak values are higher for the thicker overcoat, and the cutoff wavelength moves to longer wavelengths. As expected, the thinner overcoat exhibits a characteristically sharper cutoff feature.

These calculations were made for 10- and 50-μm-thick layers of alumina particles. The alumina particles in the overcoat had a mean particle diameter of 0.5 μm. The measurements were made at room temperature using a Perkin-Elmer Lambda-9 spectrophotometer.

Applications

The present study uses existing flow and heat-transfer models and simulations to predict the surface heat flux rates in the parametric calculations. For a specific application, the most appropriate coatings can be identified from parametric calculations made with the flow decoupled from the surface heat transfer. Allowing more realistic boundary conditions by allowing heat transfer through the material beneath the surface, a nonadiabatic boundary, and surface catalytic effects will increase the accuracy and the complexity of this approach. The surface properties predicted by this model can be easily input into an external flow code in tabular form after the initial parametric runs indicate the optimal coating for the application. The model developed in this paper can be used in parametric studies to evaluate potential overcoat and substrate materials, as well as geometric parameters such as the particle size or overcoat thickness, before producing or testing any sample materials in the laboratory.

Selective reflector overcoats are well suited to applications in which radiation is the predominant mode of heat transfer to a surface. The example shown in Fig. 7 for moderate surface heat-flux levels shows that the surface temperature of a surface exposed to radiation having a peak wavelength at the solar radiation peak of 0.5 μm was reduced by hundreds of degrees by the presence of an overcoat. These calculations represent idealized conditions for selectively reflective overcoats: short-wave radiation accounts for a high percentage of the total heating, and the total heat load remains below the ablation limit for the overcoat.

A second application is that of a high-temperature spectrometer. The radiative heat flux to a surface exposed to convective and radiative heating can be determined using a relatively small set of temperature measurements. The procedure is as follows: the total heating load is determined by temperature measurements made on the RCG coating. If the peak wavelength for the radiation and the convective heat flux are known, Fig. 7 or its equivalent for the optimized coating is used to estimate the level of the radiative heat flux. If the levels of radiative and convective heat fluxes are known instead, Fig. 8 is used to identify the peak wavelength of the incident blackbody radiation. Figures 5 and 6 are then used iteratively to characterize the peak wavelength of the incident radiation. Given less prior knowledge of the energy flux, especially in the case of incident radiation without the characteristic shape of a blackbody distribution, a larger set of measurements is required to build a high-temperature spectrometer capable of determining the spectral distribution of the radiation influx to a surface.

Figures 11–13 present design curves for making initial estimates of potential selectively reflective overcoats. This method can be used to narrow down the possible overcoat and substrate materials, particle sizes, and overcoat layer thicknesses before detailed calculations are made. Full calculations from Mie theory are strongly recommended before final conclusions are drawn, because of three

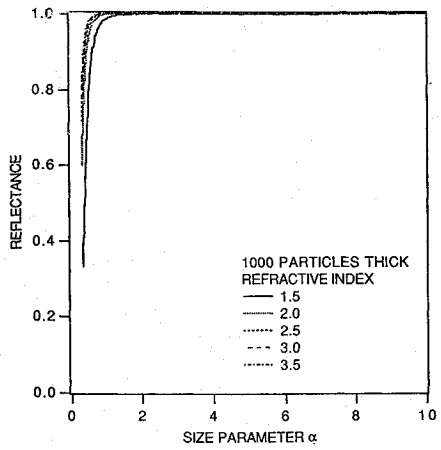

Fig. 13 Comparison of five refractive indices for 1000-particle-thick overcoats.

significant simplifying assumptions implicit in using Figs. 11–13. These three assumptions are considering a limited number of carefully selected wavelength bands for a rough estimate, neglecting absorption, and using interpolations for the refractive index or different particle sizes. The validity of the choice of wavelengths considered for the material and application of interest depends on the user's judgement. Neglecting absorption may introduce significant error at wavelengths where absorption is strong. In the highly oscillatory regions, such as in Fig. 11 at wavelengths below 2 μm, interpolation is difficult. These calculations were made for a typical particle size of 1 μm, and using a different particle size gives small oscillations imposed on the overall shape of these curves, which dampen as the underlying curve straightens out. For example, the reflectance for 10- and 100-particle-thick layers of 10-μm-diam particles oscillated with an amplitude of roughly 0.01 to 0.05 about the reflectance for 10- and 100-particle-thick layers of 1-μm-diam at a size parameter of 5 for an index of refraction of 2.0. To use these figures, the following steps are taken. The wavelengths of the most significant incident radiation or thermal radiation over which the refractive index does not vary strongly are selected. The optical properties for the wavelength and temperature of interest are used to interpolate between the appropriate curves in Figs. 11–13. The particle size for a given layer thickness is calculated from the size parameter and the wavelength. Because many independent parameters influence the effective overall optical properties of a selectively reflective overcoat, it is not possible to present a simple normalized result to estimate the final temperature reduction attainable with this strategy. Therefore, Eqs. (19–22) are used to compute the surface temperature for the radiative and convective heat flux conditions of the application of interest.

Summary

The geometric and material properties of particulate ceramic overcoats on an opaque substrate were used to calculate the total radiative properties of the surface as a function of the spectral distribution of the incident radiation and the surface temperature. The reflectance of the surface to incident radiation depends on the spectral distribution of the incident radiation. The incident radiation was assumed to exhibit the spectral distribution characteristic of a blackbody, but was scaled to give the required surface radiative heat flux. This idealization of the spectral distribution of the incident radiation allows a direct comparison of the thermal response of a surface to incident radiation having a spectral distribution representative of many problems, although it is not a realistic representation of shock-layer radiation. The spectral reflectance properties were used to calculate the reflectance and resulting total emittance of the coated surface to incident radiation. A comparison is shown between the surface temperatures of coated surfaces having different total reflectances depending on the incident radiation, and a surface having a constant reflectance.

The parameters governing the radiative properties of a particulate overcoat on a substrate can be divided into two categories: the material optical properties, through the complex index of refraction m, which depends upon the material, purity, temperature, and wavelength; and the geometric properties of the layer, i.e., the particle size d, the solid volume fraction f_v, and the layer thickness l. The approach is limited by the accuracy to which these parameters are known.

Selectively reflective overcoats can be used to significantly reduce the temperature of a heated surface under conditions where short-wavelength radiation is the predominant mode of heat transfer to a surface and the total heating is below the melting or ablation limit. In addition, these overcoats can be used to detect and characterize radiation.

References

[1]Pitts, W. C., and Murbach, M. S., "Thermal Design of Aeroassisted Orbital Transfer Vehicle Heat Shields for a Conical Drag Brake," *Journal of Spacecraft and Rockets*, Vol. 23, No. 4, 1986, pp. 442–448.

[2]Walberg, G. D., Siemers, P. M., Calloway, R. L., and Jones, J. J.,"The Aeroassist Flight Experiment," 38th International Astronautical Federation Congress, IAF Paper 87-197, Oct. 1987.

[3]Walberg, G. D., "A Review of Aerobraking for Mars Missions," 39th Congress of the International Astronautical Federation, IAF Paper 88-196, Oct. 1988.

[4]Davy, W., Park, C., Arnold, J. O., and Balakrishnan, A., "Radiometer Experiment for the Aeroassist Flight Experiment," AIAA Paper 85-0967, June 1985.

[5]Stewart, D. A., Goldstein, H. E., and Leiser, D. B., "High Temperature Glass Thermal Control Structure and Coating," United States Patent 4381333, April 26, 1983.

[6]McClure, D. J., "Durable Thin Film Coatings for Reflectors Used in Low Earth Orbit," Society of Vacuum Coaters Paper A89-33150, April 1989.

[7]Chandrasekhar, S., *Radiation Transfer*, Dover, New York, 1960.

[8]Kerker, M., *The Scattering of Light and Other Electromagnetic Radiation*, Dover, New York, 1981.

[9]Siegel, R., and Howell, J. R., *Thermal Radiation Heat Transfer*, 2nd ed., McGraw-Hill, New York, 1981.

[10]Bohren, C. F., and Huffman, D. R., *Absorption and Scattering of Light by Small Particles*, Wiley-Interscience, New York, 1983.

[11]Truelove, J. S., "The Two-Flux Model for Radiative Transfer with Strongly Anisotropic Scattering," *International Journal of Heat and Mass Transfer*, Vol. 27, No. 3, 1984, pp. 464–466.

[12]Chen, J. C., and Churchill, S. W., "Radiant Heat Transfer in Packed Beds," *AIChE Journal*, Vol. 9, No. 1, 1963, pp. 35–41.

[13]Brewster, M. Q., and Tien, C. L., "Radiative Transfer in Packed Fluidized Beds: Dependent Versus Independent Scattering," *Journal of Heat Transfer*, Vol. 104, No. 4, 1982, pp. 573–579.

[14]Drolen, B. L., "Radiative Transfer with Scattering from Closely-Spaced Spheres," Ph.D. Thesis, Univ. of California at Berkeley, Berkeley, CA, 1986.

[15]Cartigny, J. D., Yamada, Y., and Tien, C. L., "Radiative Transfer with Dependent Scattering by Particles: Part 1—Theoretical Investigation," *Journal of Heat Transfer*, Vol. 108, No. 3, 1986, pp. 608–613.

[16]Drolen, B. L., Kumar, S., and Tien, C. L., "Experiments on Dependent Scattering of Radiation," AIAA Paper 87-1485, June 1987.

[17]Kumar, S., and Tien, C. L., "Dependent Scattering and Absorption of Radiation by Small Particles," *Journal of Heat Transfer*, Vol. 112, No. 1, 1990, pp. 178–185.

[18]Kumar, S., and Tien, C. L., "Effective Diameter of Agglomerates for Radiative Extinction and Scattering," *Combustion Science and Technology*, Vol. 66, No. 6, 1989, pp. 199–216.

[19]Palik, E. D. (ed.), *Handbook of Optical Constants of Solids*, Academic Press, New York, 1985, pp. 749–763.

[20]Malitson, I. H., "Refraction and Dispersion of Synthetic Sapphire," *Journal of the Optical Society of America*, Vol. 52, No. 12, 1962, pp. 1377–1383.

[21]Touloukian, Y. S., and DeWitt, D. P., *Thermophysical Properties of Matter*, Vol. 8, Plenum Press, New York, 1972, pp. 417–425.

[22]Driscoll, W. G. (ed.), *Handbook of Optics*, Optical Society of America, McGraw-Hill, New York, 1978.

[23]Parry, D. L., and Brewster. M. Q., "Optical Constants of Al_2O_3 Smoke in Propellant Flames," *Journal of Thermophysics and Heat Transfer*, Vol. 5, No. 2, 1991, pp. 142–149.

[24]Toon, O. B., and Pollack, J. B., "The Optical Constants of Several Atmospheric Aerosol Species: Ammonium Sulfate, Aluminum Oxide, and Sodium Chloride," *Journal of Geophysical Research*, Vol. 81, No. 33, 1986, pp. 5733–5748.

[25]Goodwin, D. G., and Mitchner, M., "Infrared Optical Constants of Coal Slags: Dependence on Chemical Composition," *Journal of Thermophysics and Heat Transfer*, Vol. 3, No. 1, 1989, pp. 53–60.